EXPERIMENTAL DEGRADATION OF FLEXIBLE BEAM CONTROL IN THE PRESENCE OF DRIVE-TRAIN NON-LINEARITIES.

Julian A. de Marchi
Jun Ma
Kevin C. Craig
Active Materials and Smart Structures Laboratory
Department of Mechanical Engineering, Aeronautical
Engineering and Mechanics
Rensselaer Polytechnic Institute
Troy, New York

ABSTRACT

The adverse effects of three primary drive-train non-linearities (stiction, compliance, backlash) on the end-tip position control of a flexible beam are shown by experiment. The experiment is performed on a specially-designed mechanical positioning test bed, which allows for the introduction of precisely-quantified measures of friction, compliance and backlash into the hub mechanism of a slewing flexible beam. A multi-input and -output model is derived and used to synthesise a linear-quadratic regulator to control the beam vibration and end-tip error via a high-torque hub servo and beam surface-mounted piezoelectric transducers. A degradation in system response is demonstrated when drive-train non-linearities are introduced to the hub mechanism.

INTRODUCTION

Mechanically-coupled drive-train mechanisms proliferate the machine-tool industry: lathes, mills and the like all utilise either rotational or translational drive mechanisms for the feeding and cutting of machine parts. The quality of the finished part is directly related to the quality of the cut: better positioning of the workpiece results in tighter specification tolerances (Dorndorf *et alii*, 1994). Positioning and turning are accomplished through the use of a variety drive-train mechanisms, such as gear reductors and lead screws; the more flexible the machine tool, the more complex its drive trains become, and the more non-linear effects such as backlash, stiction and compliance will compromise its tooling quality (Mason, 1994). This is especially true of mini- and micro-machine tools currently under development for use within the evolving small-scale computer-integrated manufacturing paradigm, whose motions are so deft that these non-linearities more adversely affect them than their larger industrial counterparts (Constance, 1991).

Backlash, friction and joint compliance are traditional nemeses of precision tooling and a traditional study in mechanical engineering. To date, our understanding of these phenomena remains limited, as does our ability to control them.

Compliance is the simplest effect to model, and in many cases can be lumped as a parameter within the system it affects; since rotating cutting tools have limited torsional stiffness (especially in the case of miniaturised machine tools), for example, drive-train compliance might be modeled in series with the compli-

ance of the tool. Cutting-tool vibration is known to adversely affect the quality of the workpiece as well as reduce the lifetime of its spindle bearings (Brandon and Al-Shareef, 1991). Adaptive control strategies have been developed for the case where the drive-train compliance is not known *a priori* or varies slowly with time (Yuh and Tissue, 1991). A more interesting case, however, arises when compliance is present in addition to other non-linear effects, which research is underway at R.P.I..

Friction is more studied in the literature (Ehrich, 1991; Friedlander and Park, 1992), and is an effect present to a significant degree in mechanical positioning systems; it is more pronounced in the slowly-moving and discrete position movement or cycling inherent to the smaller, more flexible machine tools currently being developed, and is therefore of particular interest. Traditionally, a dithered control signal is used to provide a mean system excitation greater than the static friction threshold (Prakah-Asante, 1992). Adaptive strategies have also been implemented for stiction (de Wit *et alii*, 1991; Tung *et alii*, 1993; Yang and Chu, 1993), but not in conjunction with other non-linearities.

Backlash is a highly non-linear effect, and has the ability to excite high-order modes in a drive-train, unlike compliance or friction; with the aforementioned present, drive-train controllability is further undermined. A number of hysteresis models have been presented for approximating backlash, but further study is advised (Macki *et alii*, 1991). Control strategies such as dithering have been applied with some success many years ago (Freeman, 1957 and 1960), but relatively little research has been pursued in this area over recent years, excepting, for example, the works of Gorinevsky *et alii* (1991) and Tao and Kokotovic (1993).

Further study of these three non-linear phenomena is necessary, and can be facilitated by experimentation on a test-bed designed to introduce precisely-quantified combinations of backlash, stiction and compliance to the drive-train system. In particular, research into the effects of combined, rather than individually-isolated, drive-train non-linearities is warranted.
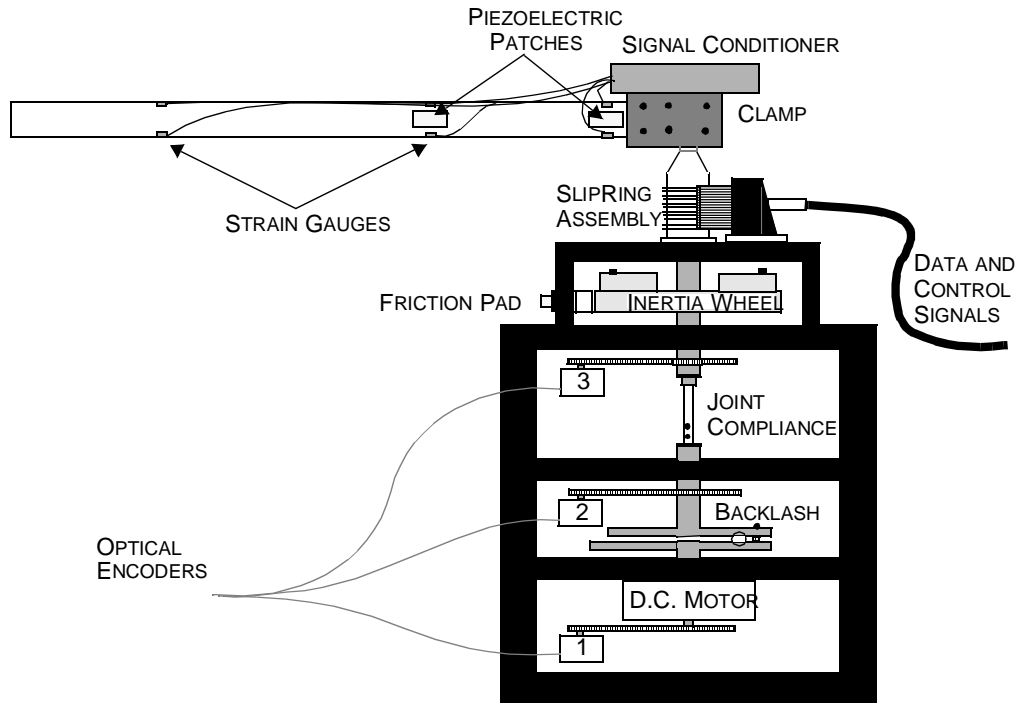
FIGURE 1: MECHANICAL POSITIONING TEST BED WITH FLEXIBLE BEAM ATTACHMENT.

MECHANICAL POSITIONING TEST-BED AT R.P.I.

The Active Materials and Smart Structures Laboratory at Rensselaer Polytechnic Institute has designed a specialised test-bed for investigating the effects of drive-train backlash, stiction and compliance, constructed by Walczyk (1991) and tested by Prakah-Asante (1992), the results of which are recently published (Prakah-Asante *et alii*, 1993). The mechanical positioning test bed at R.P.I. is specially designed to facilitate investigation of the effects of stiction, compliance and backlash in machinery (see preceding figure 1). Arbitrary combinations of these three parameters can be mimicked over a continuous range of values. Specific machine tools can be examined by affixing them to the rotating spindle on the test bed, and sensor and actuator signals linked via a 12-channel slip ring to a dedicated computer for data-acquisition and control purposes. A detailed description of the test bed can be found in the references by Walczyk (1991) and (Prakah-Asante *et alii* (1993).

SYSTEM MODEL DESCRIPTION
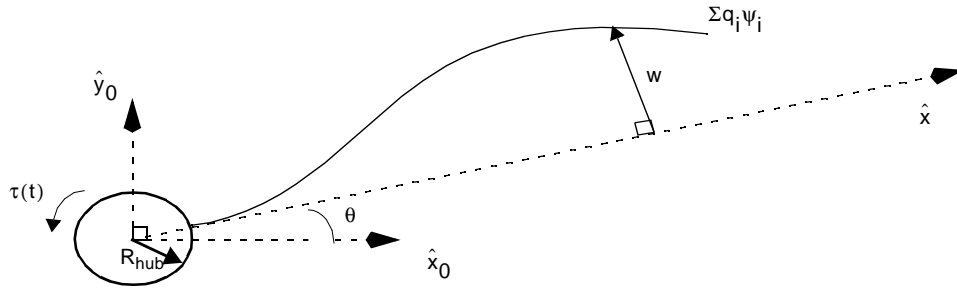
FIGURE 2: SYSTEM COORDINATES.

EQUATION OF MOTION

An arbitrary point along the beam has a differential mass $\rho_{beam}dx$ and inertial coordinates given by

$$x_0(R_{hub} + x, t) = x\cos\theta(t) - w(R_{hub} + x, t)\sin\theta(t)$$
$$y_0(R_{hub} + x, t) = x\sin\theta(t) + w(R_{hub} + x, t)\cos\theta(t)$$
$$\tag{1}$$

Its inertial velocity is

$$\dot{x}_0 = -[(R_{hub} + x)\dot\theta + \dot{w}]\sin\theta - \dot\theta w\cos\theta$$
$$\dot{y}_0 = [(R_{hub} + x)\dot\theta + \dot{w}]\cos\theta - \dot\theta w\sin\theta$$
$$\tag{2}$$

Summing the square of each component, the cross terms cancel and the kinetic energy of the beam is

$$T_{beam} = \frac{1}{2}\int_0^{l_{beam}} \rho_{beam}(\dot{x}_0{}^2 + \dot{y}_0{}^2)dx = \frac{1}{2}\int_0^{l_{beam}} \rho_{beam}\left\{[(R_{hub} + x)\dot\theta + \dot{w}]^2 + (\dot\theta w)^2\right\}dx$$
$$= \frac{1}{2}\left\{I_{beam}\dot\theta^2 + \int_0^{l_{beam}} \rho_{beam}[\dot{w}^2 + 2(R_{hub} + x)\dot{w}\dot\theta + (w\dot\theta)^2]dx\right\}$$
$$\tag{3}$$

beam length:	l_{beam}	(L)	PZT length:	l_{PZT}	(L)
beam width:	w_{beam}	(L)	PZT width:	w_{PZT}	(L)
beam thickness:	t_{beam}	(L)	PZT thickness:	t_{PZT}	(L)
beam density:	ρ_{beam}	(ML^{-3})	PZT surface area:	$A_{PZT} = (lw)_{PZT}$	(L^2)
beam elasticity:	E_{beam}	$(ML^{-1}T^{-2})$	PZT elasticity:	E_{PZT}	$(ML^{-1}T^{-2})$
strain:	$\varepsilon(x, t)$	$(\bullet)$	PZT moment:	$M_{PZT}(x, t)$	(MLT^{-2})
beam moment:	I_{beam}	(ML^2)	bond "strength":	E_{bond}	$(ML^{-1}T^{-2})$
cross-section:	A_c	(L^2)	bond thickness:	t_{bond}	(L)
hub torque:	$\tau_{hub}(t)$	(MLT^{-2})	beam area inertia:	I_c	(L^4)
hub moment:	i_{hub}	(ML^2)	hub radius:	R_{hub}	(L)
total moment:	$I_{tot} = I_{hub} + I_{beam}$	(ML^2)	radial displacement:	x	(L)
angle:	$\theta(t)$	(radians)	beam deflection:	$w(x, t)$	(L)
static friction:	μ_{static}	(ML^2)	modal eigenvalue:	α_i	(L^{-1})
dynamic friction:	$\mu_{dynamic}$	(ML^2)	modal eigenshape:	$\psi_i(x)$	$(\bullet)$
viscous friction:	$\nu_{viscous}$	(ML^2T)	modal participation:	$q_i(t)$	$(\bullet)$
motor command:	$V_{motor}(t)$	(V)	motor torque const.:	k_{motor}	$(MLT^{-2}A^{-1})$
PZT command:	$V_i(t)$	(V)	amplifier constant:	k_{amp}	(AV^{-1})
gauge excitation:	$V_{gauge}(t)$	(V)	back-EMF constant:	k_{EMF}	(ML^2T)
gauge constant:	$k_{gauge}(t)$	(V^{-1})	PZT constant:	k_{PZT}	$(ML^3T^{-2}V^{-1})$
$\frac{d\square}{dx}$:	$\square'$	$(D_{spacial})$	$\frac{d\square}{dt}$:	$\square$	$(D_{temporal})$

The potential energy of the system is governed by the strain energy of the beam during bending (Gere and Timoshenko, 1984), which is, assuming small deflections $w(x, t)$,

$$V_{beam} = \frac{1}{2}\int_0^{l_{beam}} E_{beam}I_c w''^2 dx \ , \tag{4}$$

where I_c is the cross-sectional area moment of the beam (units L^4), assuming that axial extensions are small during bending, which is reasonable, since the width of the beam is small with respect to its length.

Adding the kinetic energy of the hub to the kinetic energy of the beam (equation (3)), the total kinetic energy of the system

$$T_{tot} = T_{hub} + T_{beam}$$
$$= \frac{1}{2}\left\{ I_{tot}\dot\theta^2(t) + (k_{motor}k_{amp}k_{EMF} + \nu_{viscous})\theta(t) + \int_0^{l_{beam}} \rho_{beam}[\dot w^2 + 2(R_{hub} + x)\dot w \dot\theta + (w\dot\theta)^2]dx \right\} \ . \tag{5}$$

Including the work done by the DC motor and PZTs,

$$W_{external} = W_{hub} + W_{PZT} = \tau_{hub}\theta + \int_0^{l_{beam}} M_{PZT}w''dx \ . \tag{6}$$

Applying either Hamilton's Principal of Least Action or Lagrange's Kinetic-Potential Equations yields the non-linear coupled equations of motion (for example, Fox, 1963)

$$\tau_{hub} = I_{tot}\ddot{\theta} + 2\rho_{beam}\int_0^{l_{beam}} [(R_{hub} + x)\ddot{w} + \dot{w}\dot{\theta} + w^2\dot{\theta}]dx \ ,$$

$$M''_{PZT} = E_{beam}I_c w^{iv} + \rho_{beam}[(R_{hub} + x)\ddot{\theta} + \dot{\theta}^2 w + \ddot{w}] \tag{7}$$

where the second term in the hub-torque equation is precisely the "flexible momentum" given by Li and Bainum (1992). We assume that the PZTs add negligible stiffness to the overall beam. Substituting equation (9) for the deflection into the equations of motion (7),

$$\tau_{hub} = I_{tot}\ddot{\theta} + 2\rho_{beam}\int_0^l [(R_{hub} + x)\ddot{\vec{q}} + \dot{\theta}\dot{\vec{q}} + \theta\dot{\vec{q}}]^T\vec{\psi}dx$$

$$M''_{PZT} = E_{beam}I_c\vec{q}^T\vec{\psi}^{iv} + \rho_{beam}[(R_{hub} + x)\ddot{\theta} + (\dot{\theta}^2\vec{q} + \ddot{\vec{q}})^T\vec{\psi}] \tag{8}$$

The beam deflection can be expressed in terms of a linear superposition of the orthogonal mode shapes $\psi_i(x)$ (eigenfunctions) with their participation factors $q_i(t)$ (generalised coordinates), as per Thomson (1993):

$$w(x,t) = \sum_{i=1}^{N_{modes}} q_i(t)\psi_i(x) = \vec{q}^T(t)\vec{\psi}(x) \ . \tag{9}$$

$q_i(t)$ denotes the temporal participation factor (relative amplitude) of mode i at time t.
The equation for the mode shape is subjected to the clamped-free beam boundary conditions

$$\psi_i(0) = \psi_i'(0) = \psi_i''(l_{beam}) = \psi_i'''(l_{beam}) = 0 \ , \tag{10}$$

which state that the angle and deflection of the beam are nil where it is clamped, and the moment and shear are nil at the end-tip of the beam. Integrating the equation of motion with respect to radial displacement x and applying the boundary conditions,

$$I_{beam}\ddot{\theta}\int_0^{l_{beam}} \rho_{beam}(R_{hub} + x)\psi_i dx + \sum_{i=1}^{N_{modes}} E_{beam}I_{beam}q_i\int_0^{l_{beam}} \psi_i''^2 + \rho_{beam}\ddot{q}_i\int_0^{l_{beam}} \psi_i^2$$

$$= \int_0^{l_{beam}} M''_{beam}\psi_i dx = M_1[\psi_i(x_{1-}) - \psi_i(x_{1+})] + M_2[\psi_i(x_{2-}) - \psi_i(x_{2+})] \tag{11}$$

MODES AND MODE PROPERTIES

It is known (Thomson, 1993) that for a prismatic beam (Gere and Timoshenko, 1984) (density ρ_{beam} and flexural rigidity $E_{beam}I_c$ constant along its length),

$$\psi_i(x) = \sin\alpha_i x - \sinh\alpha_i x + \frac{\sin\alpha_i l_{beam} + \sinh\alpha_i l_{beam}}{\cos\alpha_i l_{beam} + \cosh\alpha_i l_{beam}}\cosh\alpha_i x - \cos\alpha_i x \quad , \tag{12}$$

where α_i satisfies $(\cos\alpha_i l_{beam}\cosh\alpha_i l_{beam} + 1) = 0$. The first four values of αl_{beam} are: {1.8751, 4.6941, 7.8548, 10.9955} (dimensionless); these can be used to compute the first four natural frequencies of a flexible beam via the relation

$$\omega_i = \alpha_i^2\sqrt{\frac{E_{beam}I_c}{\rho_{beam}A_c}} = \alpha_i^2 t_{beam}\sqrt{\frac{E_{beam}}{\rho_{beam}}} \qquad i \in [1, N_{modes}] \quad . \tag{13}$$

Other beam properties are derived using linear beam theory (small deflections are assumed). Since we are using strain gauges as our feedback sensors, the beam normal strain is also of interest, and is given by:

$$\varepsilon_{normal}(x, t) = \frac{M(x, t)t_{beam}}{2E_{beam}I_c} \quad . \tag{14}$$

where the beam moment

$$M(x, t) = E_{beam}I_c w''(x, t) = E_{beam}I_c \vec{q}^T(t)\vec{\psi}''(x) \quad , \tag{15}$$

with

$$\psi''_i(x) = \alpha_i^2\left[-(\sin\alpha_i x + \sinh\alpha_i x) + \frac{\sin\alpha_i l_{beam} + \sinh\alpha_i l_{beam}}{\cos\alpha_i l_{beam} + \cosh\alpha_i l_{beam}}(\cos\alpha_i x + \cosh\alpha_i x)\right] \quad . \tag{16}$$

Combining equations (14) and (15) above,

$$\vec{q}^T(t)\vec{\psi}''(x_i) = \frac{2\varepsilon_{normal}(x_i, t)}{t_{beam}} \quad , \tag{17}$$

here the measured value

$$\varepsilon_{normal}(x_i, t) = (kV(t))_{gauge(i)} \tag{18}$$

of the strain gauge about x_i. Imposing orthogonality with Kronecker Delta Function $\delta_{\psi(x)}$ such that

$$\psi_j^{(n)}(x)\sum_{i=1}^{N_{modes}} \square_j(t)\psi_i^n(x) = \square_i(t)\delta_{\psi(x)} = \left\{\begin{array}{cc} 0 & \forall(i \neq j) \\ \psi_j^{(n)}(x)\square_j(t)_j\psi_j^{(n)}(x) & (i = j) \end{array}\right\} = \square_{jj} \quad , \tag{19}$$

makes matrices J_{beam} , C_{beam} , K_{beam} and F_{PZT} pure diagonal. One can readily verify via equation (13) that

$$\omega_i^2 = \frac{K_{ii}}{J_{ii}} \ . \tag{20}$$

COMBINED STATE-SPACE FORMULATION

The system model is reduced to second order and can thus be written as

$$J\ddot{\vec{y}} + C\dot{\vec{y}} + K\vec{y} = F\vec{u} \ , \tag{21}$$

where combining equations (17) and (20) yields respective state and control vectors

$$\vec{y} = \begin{bmatrix} \theta(t) \\ \vec{q}(t) \end{bmatrix} = \begin{bmatrix} \theta(t) \\ q_1(t) \\ \vdots \\ q_{N_{modes}}(t) \end{bmatrix}_{(1+N_{modes})x1} \qquad \vec{u} = \begin{bmatrix} V_{motor}(t) \\ \vec{V}_{PZT}(t) \end{bmatrix} = \begin{bmatrix} V_{motor}(t) \\ V_1(t) \\ \vdots \\ V_{N_{PZT}}(t) \end{bmatrix}_{(1+N_{PZT})x1} \quad ; \tag{22}$$

and where block-diagonal J , C , K and F represent the combined mass/inertia, damping, stiffness and forcing matrices respectively, as below:

$$J = \begin{bmatrix} I_{tot} & \int_0^{l_{beam}} \rho_{beam}(R+x)\psi_1 dx & \ldots & \int_0^{l_{beam}} \rho_{beam}(R+x)\psi_{N_{modes}} dx \\ \int_0^{l_{beam}} \rho_{beam}(R+x)\psi_1 dx & \int_0^{l_{beam}} \rho_{beam}\psi_1^2 dx & \ldots & \int_0^{l_{beam}} \rho_{beam}\psi_{N_{modes}}\psi_1 dx \\ \vdots & \vdots & & \vdots \\ \int_0^{l_{beam}} \rho_{beam}(R+x)\psi_{N_{modes}} dx & \int_0^{l_{beam}} \rho_{beam}\psi_1\psi_{N_{modes}} dx & \ldots & \int_0^{l_{beam}} \rho_{beam}\psi_{N_{modes}}^2 dx \end{bmatrix}_{(1+N_{modes})^2} \tag{23}$$

$$C = \begin{bmatrix} k_{motor}k_{EMF} + v_{viscous} & 0 \\ 0 & 0 \end{bmatrix}_{(1+N_{modes})^2} \ ; \tag{24}$$

$$K = \begin{bmatrix} 0 & 0 & \ldots & 0 \\ 0 & \int_0^{l_{beam}} (EI)_{beam}\psi''^2_1 dx & \ldots & \int_0^{l_{beam}} (EI)_{beam}\psi''_1\psi''_{N_{modes}} dx \\ \vdots & \vdots & & \vdots \\ 0 & \int_0^{l_{beam}} (EI)_{beam}\psi''_{N_{modes}}\psi''_1 dx & \ldots & \int_0^{l_{beam}} (EI)_{beam}\psi''^2_{N_{modes}} dx \end{bmatrix}_{(1+N_{modes})^2} \ ; \tag{25}$$

and

$$F = \begin{bmatrix} k_{motor}k_{amp} & 0 & \cdots & 0 \\ 0 & k_{PZT}\psi'_1 x_{1-} - \psi'_1 x_{1+} & \cdots & k_{PZT}\psi'_1 x_{N_{PZT}-} - \psi'_1 x_{N_{PZT}+} \\ \vdots & \vdots & & \vdots \\ 0 & k_{PZT}\psi'_{N_{modes}} x_{1-} - \psi'_{N_{modes}} x_{1+} & \cdots k_{PZT}\psi'_{N_{modes}} x_{N_{PZT}-} - \psi'_{N_{modes}} x_{N_{PZT}+} \end{bmatrix} .$$

(26)

$$= \begin{bmatrix} k_{motor}k_{amp} & 0 \\ 0 & k_{PZT}\left[\vec{\psi}'(x_{1-}) - \vec{\psi}'(x_{1+}) \ \ \vec{\psi}'\left(x_{N_{PZT}-}\right) - \vec{\psi}'\left(x_{N_{PZT}+}\right) \right]_{N_{modes} \times N_{PZT}} \end{bmatrix}$$

Allow a modified state vector $\vec{x} = \begin{bmatrix} \vec{y} & \dot{\vec{y}} \end{bmatrix}^T$. such that $\dot{\vec{x}} = A\vec{x} + B\vec{u}$; then the corresponding state-space matrix A is diagonalisable using first-order theory:

$$A = \begin{bmatrix} O & I \\ -J^{-1}K & -J^{-1}C \end{bmatrix}_{[2(1+N_{modes})]^2} \quad \text{and} \quad B = \begin{bmatrix} O \\ J^{-1}F \end{bmatrix}_{2(1+N_{modes}) \times (1+N_{PZT})} .$$

(27)

SIMULATION RESULTS

Control is implemented in linear quadratic regulator form (see figure 3 below) with a typical performance index seeking to minimise the weighted squares of the state and input vectors:

$$J = \sum (\vec{y}^T Q\vec{y} + \vec{u}^T R\vec{u}) \ ,$$

(28)

where matrices Q and R are pure diagonal and represent the relative weights of states $\vec{y}$ and controls $\vec{u}$, respectively. The system response is simulated for a step input as well as sinusoidal and square disturbance inputs (figures follow). In each case the disturbance is already present when the control is activated.
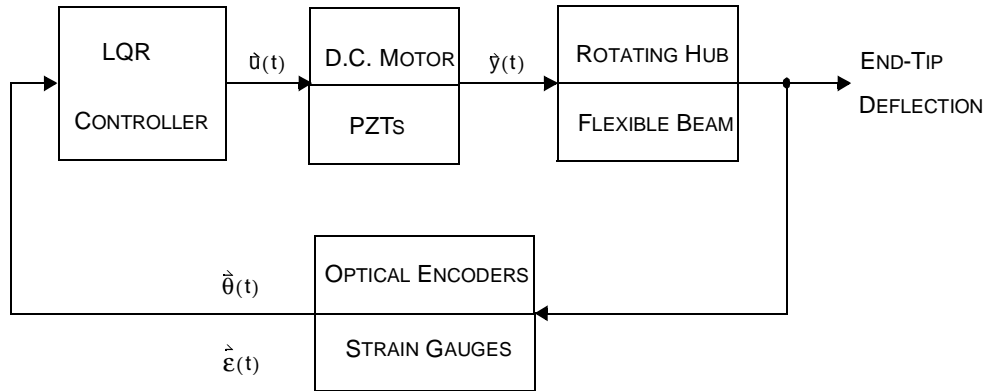
FIGURE 3: LINEAR-QUADRATIC REGULATOR BLOCK DIAGRAMME.

WITH PZTs

WITHOUT PZTs

FIGURE 4: Step Response with and Without PZT Control.

WITH PZTs

WITHOUT PZTs

FIGURE 5: Sinusoidal Response with and without PZT Control.

WITH PZTs

WITHOUT PZTs

WITH PZTs

WITHOUT PZTs

FIGURE 6: SQUARE-WAVE RESPONSE WITH AND WITHOUT PZT CONTROL.

STEADY-STATE DISTURBANCE

WITHOUT PZTs

WITH PZTs

FIGURE 7: COMBINED STEP AND DISTURBANCE RESPONSE WITH AND WITHOUT PZT CONTROL.

Notice that the end-tip deflection from the rigid-body axis is significantly reduced using the PZT patches. The damping can be improved even more, as long as the PZT break-down voltage is observed. The simulations are verified with experimental results in the following sections.

OPTIMAL TRANSDUCER PLACEMENT

The beam is actuated by two pairs of PZT patches, each co-located with one another and placed symmetrically about the longest principal axis of the beam. In this configuration, flexure alone can be directly controlled, not torsion. By applying the inverse command voltage at one patch to its co-located partner, the PZT-induced moment of the beam about that point x_i will be doubled. Since piezoceramic actuation is bounded by a maximum break-down voltage, at which point the dielectric no longer insulates the PZT poles (the act of "de-polarisation", as per Yuh and Tissue, 1991), co-locating actuator pairs doubles beam-moment transduction with no additional actuation effort. Although co-location of the piezoelectric actuators is not *per se* necessary for the case of a thin beam, it is also useful when one of a pair of PZT patches is used for strain-rate sensing while the other is used for actuation; note that this method yields no additional bending moment, but does allow direct measurement of the beam strain rate $\dot{w}''(x_i, t)$.

The beam strain energy is sensed using twelve strain gauges co-located about its longest principal axis, two of which are co-located with positions x_i of the PZT patches $i \in \{1, 2\}$, and the last one with a position $x_{i=3}$ corresponding to relatively large strains over the first four modes, as explained in detail below. Since these sensors convey strain, which is also directly caused by beam bending, their positions along the beam should coincide with those of the actuators purely to satisfy observability requirements; however, it is also necessary to co-locate the sensors with the actuators for full-state feed-back control. The third set of strain gauges augments the feed-back information but is not required, although it should be noted that with discretely-located actuators and sensors such as we use here, the degree of controllability of the flexible beam certainly increases when more sensor-actuator pairs are placed along its length.

Choice of the location of the actuators is restricted by the controllability requirement that none be placed at a flexural node; in fact, it is optimal to place the patches where flexural maxima can be expected. In particular, these locations are determined by superposition of the longitudinal surface strain ε (proportional to the bending moment) along the beam due to the first N modes of interest, which can be calculated from the mode shapes via the relation

$$\varepsilon_i(x_i, t) = \frac{1}{2}t_{b+p}(x_i)K(x_i, t) = \frac{1}{2}t_{b+p}(x_i)\frac{M_i(x_i, t)}{E_{b+p}I_{b+p}} \quad , \tag{29}$$

where $\kappa_i(x, t)$ is the beam curvature at sensor position x_i and time t ; note that this can only be measured where sensors are placed. Note also that the thickness, modulus and inertia about x_1 and x_2 differ from that about x_3 and elsewhere along the beam, due to the fact that the PZTs are stiff ceramics (the subscript $\square_{b+p}$ denotes the combined property of the beam and mounted patch at x_i). We assume that the thickness and stiffness of the PZTs have a negligible effect on those of the plain beam itself ($\square_{b+p} \approx \square_b$). The beam moment $M(x, t)$ can be computed theoretically from the deflection via equation (15).

Although this accounts for the simultaneous presence of a number of modes during residual beam vibration, unfortunately there is no way of knowing *a priori* the relative individual contribution (represented by the modal participation factor $q_i(t)$) of each of the modes, whose excitability really depends a great deal on the range of excitation frequencies expected in the beam. We elect here to control only the first three modes, under the following assumptions: *(i)* modes higher than the first contribute asymptotically negligible energy to the beam for our actuation bandwidth (we therefore treat only the first three modes); *(ii)* the maxima of the un-normalised mode shapes themselves are each representative of that mode's participation factor. The first four mode shapes and associated bending moments are shown individually and superimposed (see the following figures); these curves are based on calculations using system parameter values defined in the Appendix. We are interested in controlling modes 1 through $N_{modes} = 3$ in this experiment, but mode 4 is also considered as an investigation into spill-over effects (the inadvertent observation and control of higher modes aliased as the modes intentionally sought to observe and control).

Final selection of the transducer locations is based on a comparison of strain maxima for both the three- and four-mode shape superpositions shown below. We strike a sub-optimal compromise between either case so that at some future stage we may compare control of three and four modes respectively using the

same equipment (because in our case the transducers are permanently affixed to the beam). Optimal transducer placement is still under study.
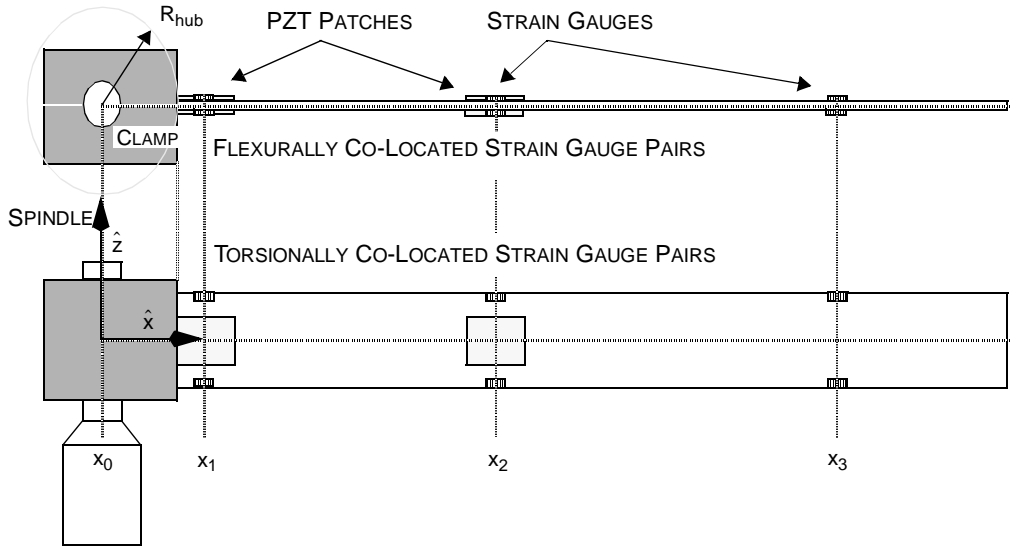
FIGURE 8: FLEXIBLE BEAM GEOMETRY.

TABLE 1: OPTIMAL SENSOR AND ACTUATOR PLACEMENT.

	Optimal Distance from Clamped End (English)	(SI)	Absolute Strain Maxima ($\mu\varepsilon$) (modes 1-3)	Optimal Distance from Clamped End (English)	(SI)	Absolute Strain Maxima ($\mu\varepsilon$) (modes 1-4)
x_1	0 in	0 cm	1794	0 in	0 cm	2422
x_2	10.85 in	27.57 cm	1326	7.780 in	19.76 cm	1696
x_3	26.57 in	67.50 cm	2444	17.91 in	45.50 cm	2291
x_4				29.72 in	75.48 cm	4357

TABLE 2: ACTUAL SENSOR AND ACTUATOR PLACEMENT.

	Actual Distance from Clamped End (English)	(SI)	Absolute Measured Strain Maxima ($\mu\varepsilon$) (modes 1-3)	Absolute Measured Strain Maxima ($\mu\varepsilon$) (modes 1-4)
x_1	1 in	2.54 cm	1380	1658
x_2	12.87 in	32.7 cm	1177	269.5
x_3	28 in	71.1 cm	2370	4003

FIGURE 9: Superposition of Flexible Beam Modes 1-3.

FIGURE 10: .Superposition of Flexible Beam Modes 1-4.

EXPERIMENTAL RESULTS

Experimental validation of the corruptive effects of stiction, backlash and compliance is performed by comparing the end-tip position and residual beam vibration responses of each case. The system response to a 10-Hz periodic square-wave disturbance is assumed to be an extrapolation of this case, with a degradation of response commensurate with faster disturbance frequencies. The following plots in this section show the average total response time of our system to be on the order of one half second when PZT patches assist in damping beam vibrations, which suggests a periodic signal of 10Hz will result in a less-robust response. In order to limit the space of this presentation, however, only the step responses are shown here.

The beam is first slewed through a 90-degree rotation, and the end-tip position and residual beam vibrations recorded. The beam is controlled in the absence of deliberate drive-train non-linearities (there exist some inherent non-controllable non-linearities in the system). Figures 11 and 12 following demonstrate the improved positioning response of the beam using an LQR control which accounts for the "flexible momentum" of the beam (flexibility is modeled); these responses are contrasted with the simplified LQR control, which ignores the non-linear coupling between the flexible beam and the drive shaft (no flexibility is assumed. A proportional+derivative controller with control parameters k_p = 0.145 V and k_d = 0.570 Vs^{-1} is used to handle the slewing motion of the motorised drive-train system, with the included rigid-body inertia of the beam, in both instances. These control parameters are derived after fine-tuning the LQR-modeled response for the actual system; note, however, that the useful range of tuning can be rather broad, depending on the desired response characteristics.

Next, the same step reference is applied, but now about 1.675 ft-lb$_f$ (~2.271 Nm) friction torque is introduced. Notice the variability in possible steady-state error using the LQR method (there is no integration by the controller since only proportional and derivative terms are in the feed-back loop). In the plot shown, the response using PZTs has no overshoot and less steady-state error. This can be attributed to the control effect on the beam as excited by the PZTs during the slewing motion. See figures 13 and 14 for plots comparing the end-tip position and residual vibrations with unmodeled friction in the drive train.

The system response to backlash is less degraded than might be expected. We attribute the smooth backlash responses shown in figures 15 and 16 to the high inertia moment of the rotating system (hub + beam). Since backlash becomes more critical towards the final positioning stage, where there are more oscillations of the hub angle about the set-point and the control effort by the hub is also less, most backlash phenomena would be the result of PZT actuation; however, the inertia of the system is too great for the PZTs to appreciably impart hub motions large enough to induce limit cycling within the hysteretic bounds of the amount of backlash configurable on the test bed (in this experiment we use the maximum of 4.0 mrad (~0.23 degrees)). As a result, the perceived backlash degradation is minimal. Please note, however, that this is likely more due to the physical characteristics of the test bed we use, and not necessarily indicative of a general trend of improved response achieved by using PZTs. This is readily confirmed by comparing the response shown following with that obtained in the absence of drive-train non-linearities. Nevertheless a small steady-state error is noticable in the backlash-corrupted end-tip response that follows, which is expected, although not nearly as degrading as the response due to friction shown on the preceding pages. As machines become more miniaturised, however, effects such as backlash can be expected to become more pronounced. Further investigation into the effects of backlash in positioning and tracking systems is currently in progress.

Response degradation due to compliance, shown in figures 17 and 18, is very prominent, and in our study represents an important deviation from the other responses. This is the only case we show where the augmented control using PZTs is worse (and significantly so) than hub control alone. Drive-train compliance introduces modal components which are directly inter-coupled with the flexible beam modes, but not included in the reference model for the LQR design. The vibrations due to drive train compliance is thus a form of spill-over, but not restricted to modes higher than those we seek to control; the end effect of this is that corruption of the lower-order modes is more likely as the compliant drive member becomes more flexible, as would be anticipated. In the case we show, the PZT response to an unmodeled 0.19 mrad / ft-lbf (~0.14 mrad / Nm) compliance is so degraded that the higher modes are barely controllable; although the hub control brings the end-tip position in the vicinity of its desired set-point, beam vibration starts a limit cycle because of the compliant drive-train member. It is worth noting that an adaptive scheme may be able to identify the equivalent shift in modal frequencies and compensate for the steady-state oscillation for a number of different reference trajectories or set-points, another subject currently under closer investigation.

No flexibility
ASSUMED

Flexibility
MODELED

FIGURE 11: Rigid-Body versus Flexible-Beam Control: End-Tip Position.

Flexibility
MODELED

No flexibility
ASSUMED

FIGURE 12: Rigid-Body versus Flexible-Beam Control: Residual Beam Strain.

WITHOUT PZTs

WITH PZTs

FIGURE 13: END-TIP POSITION UNDER FRICTION.

WITH PZTs

WITHOUT PZTs

FIGURE 14: RESIDUAL BEAM STRAIN UNDER FRICTION.

WITH PZTs

WITHOUT PZTs

FIGURE 15: End-Tip Position under Backlash.

WITHOUT PZTs

WITH PZTs

FIGURE 16: Residual Beam Strain under Backlash.

WITH PZTs

WITHOUT PZTs

FIGURE 17: END-TIP POSITION UNDER COMPLIANCE.

WITH PZTs

WITHOUT PZTs
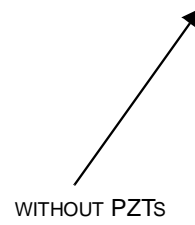
FIGURE 18: RESIDUAL BEAM STRAIN UNDER COMPLIANCE.

CONCLUSIONS

We have demonstrated the efficacy of surface-mounted piezoelectric patches for residual vibration suppression in a flexible beam. However, degradation of the positioning response of flexible structures is also clearly demonstrated when drive-train non-linearities are introduced. Particularly important is the observation that as controller optimisation based on a reference model is increased, the likelihood of instabilities due to inherent and unmodeled system non-linearities also increases, as expected. It is also shown that particular system configurations may result in either a satisfactory or more corrupted response, depending on the individual influences of particular drive-train non-linearities such as friction, backlash and compliance.

FUTURE TEST-BED RESEARCH

Machine tools experience similar effects to those demonstrated in this paper: compliance, friction and backlash are common in these tools. The range of modeling flexibility built into the R.P.I. research test bed shows promise that extrapolations of even micro-machine tool dynamics may be duplicated accurately to scale for close examination and control of the kinds of degrading effects also common to many machine tools. A number of experimental methods and non-linear controller designs have already been tested and verified using the test-bed (Prakah-Asante, 1992; Prakah-Asante *et alii*, 1993). Future work includes on-line identification and adaptive control of machine tool positioning under the effects of backlash, stiction and compliance. Traditional as well as modern controller designs, potentially driving novel control actuators, will be implemented as part of the National Science Foundation's Machine-Tool Research Initiative. Automated diagnostics quantifying and tracking ambient non-linear drive-train components during normal operation are being developed. Further work on the optimal placement of beam-mounted transducers is under investigation, and the further application of smart technologies, *exempli gratia* fibre-optic strain gauges and piezoelectric stack actuators, is also being considered. The Active Materials and Smart Structures Laboratory at R.P.I. is currently committed to continued research into vibration suppression and noise cancellation strategies for a variety of "intelligent" structures and controller frameworks.

ACKNOWLEDGMENTS

APPENDIX: SYSTEM SPECIFICATIONS

TABLE A: Test Bed Parameters

Description	Value (English)	Value (SI)
clamp radius (R_{hub})	2-$\frac{1}{4}$ in.	~ 5.7 cm
Clamp Moment (I_{hub})	9.802×10^{-4} ft-lb$_f$-s^2	1.329×10^{-3} Nms^2
Motor Moment (I_{motor})	5.8333×10^{-4} ft-lb$_f$-s^2	7.9089×10^{-4} Nms^2
Spindle Moment (I_{drive})	1.732 ft-lb$_f$-s^2	2.348 Nms^2
Dynamic Friction ($\mu_{dynamic}$)	0.0234 ft-lb$_f$	~ 0.03175 Nm
Static Friction (μ_{static})	0.0817 ft-lb$_f$	~ 0.11075 Nm
Viscous Friction ($\nu_{viscous}$)	0.3243 ft-lb$_f$-s	~ 0.4397 Nms

TABLE B: BEAM FLEXURAL FREQUENCIES.

Mode n	ω_n (rad/s)	f_n (Hz)
fundamental	179π	89.6
second	1120π	562
third	3150π	1570
fourth	6160π	3080

TABLE C: FLEXIBLE BEAM PROPERTIES.

Description	Value (English)	Value (SI)
material	6061-T6 Al (Aluminium alloy)	
mass density (ρ_{beam})	5.2 slug / ft^3	2.7 Mg / m^3
modulus (E_{beam})	10 Msi	70 GPa
length (l_{beam})	38-$^1/_2$ in.	~ 97.8 cm
width (w_{beam})	2 in.	~ 5.1 cm
thickness (t_{beam})	$^1/_8$ in.	~ 32 mm
cross-sectional inertia (I_c)	0.83 in.^{4}	~ 3.5 cm^4
moment ($I_{beam/spindle}$)	17 slug-in.^{2}	~ 0.16 Nms^2
PZT constant (k_{PZT})	2.221 x10-3 ft^2-lb$_f$ / V	0.9178 x10^{-3} Nm^2 / V
gauge constant (k_{gauge})	0.2370 / V	

TABLE D: DC MOTOR SPECIFICATIONS.

Specification	Value (English)	Value (SI)
Manufacturer and Model	P.M.I. Motion Technologies U16M4T Servodisc	
Total Resistance (R_{motor})	1.62 Ω	
Total Inductance (H_{motor})	< 100.0 μH	
Back EMF Constant (k_{EMF})	0.2053 Vs	
RMS (Peak) Current ($i_{max(motor)}$)	10.78 (94.9) A	
RMS (Peak) Torque ($\tau_{max(motor)}$)	1.5005 (14.315) ft-lb$_f$	~ 2.0344 (19.408) Nm
Motor Torque Constant k_{motor}	0.1515 ft-lb$_f$ / A	0.2054 Nm / A
Moment (I_{motor})	5.8333 x10^{-4} ft-lb$_f$-sec^2	7.9089 x10^{-4} Nms^2

TABLE E: Motor Amplifier Specifications.

Specification	Value (English)	Value (SI)
Manufacturer and Model	P.M.I. Motion Technologies AXA-180-10-20 Servo Amplifier	
Amplifier Constant (k_{amp})	0.9975 ± 0.0325 A / V	
RMS (Peak) Current ($i_{max(amp)}$)	7.368 (19.57) A	
Corresponding RMS (Peak) Motor Torque	1.116 (2.965) ft-lb$_f$	1.5134 (4.0197) Nm

TABLE F: Computer Control Specifications.

Specification	Value (English)	Value (SI)
Manufacturer and Models	National Instruments Lab-PC+ and AT-AO-6	
Command Resolution (ρ_{comm})	± 0.025 % (12-bit DAC)	
Peak (RMS) Voltage Range ($v_{max(comm)}$)	± 10 ($\pm 7.386 \pm 0.240$) V@ 2 mA	
Peak Current Range ($i_{max(comm)}$)	$\pm 9.975 \pm 0.325$ A	
Peak Torque Range ($\Delta\tau_{motor}$)	$\pm 1.511 \pm 0.049$ ft-lb$_f$	$\pm 2.049 \pm 0.067$ Nm

REFERENCES

Brandon J.A. and Al-Shareef K.J.H. , 1991: "On the Applicability of Modal and Response Representations in the Dynamic Analysis of Machine Tool Spindle Bearing Systems." *Proceedings of the Institute of Mechanical Engineers*, vol.205 pp.139-145.

Constance J., 1991: "Intelligent Processing of Materials." *Mechanical Engineering*, (Nov.) pp.37-40.

Dorndorf U., Kiridena V.S.B., and Ferreira P.M., 1994: "Optimal Budgeting of Quasistatic Machine Tool Errors." *Journal of Engineering for Industry*, vol.116 (Feb.) pp.42-53.

Ehrich N.E. (Krishnaprasad P.S.), 1991: "An Investigation of Control Strategies for Friction Compensation." *The University of Maryland Department of Electrical Engineering,* Master of Science Thesis.

Fox C., 1963: An Introduction to the Calculus of Variations, corr.ed. (Dover).

Freeman E.A., 1957: "An Approximate Transient Analysis of a Second-Order Position-Control System when Backlash is Present." *The Institution of Electrical Engineers*, Monograph no.254M (Sep.).

Freeman E.A., 1960: "The Stabilisation of Control Systems with Backlash using a High-Frequency On-Off Loop." *The Institution of Electrical Engineers*, Monograph no.354M (Feb.).

Friedlander B. and Park Y-J., 1992: "On Adaptive Friction Compensation." *IEEE Transactions on Automatic Control*, vol.37 no.10 (Oct.) pp.1609-1612.

Gere J.M. and Timoshenko S.P., 1984: Mechanics of Materials, ed.3 (PWS-Kent).

Gorinevsky D.M., Lensky A.V., and Sabitov E.I., 1991: "Feedback Control of a One-Link Flexible Manipulator with Gear Train." *Journal of Robotic Systems*, vol.8 no.5 (Oct.) pp.659-676.

Li Z. and Bainum P.M., 1992: "Vibration Control of Flexible Spacecraft Integrating a Momentum-Exchange Controller and a Distributed Piezoelectric Actuator." *Third International Conference on Adaptive Structures*, Nov.

Macki J.W., Nistri P., and Zecca P., 1993: "Mathematical Models for Hysteresis." *Society for Industrial and Applied Mathematics Review*, vol.35 no.1 (Mar.) pp.94-123.

Mason F., 1994: "Multipart Fixturing Delivers Speed and Flexibility." *American Machinist*, (Jan.) pp.51-

53.

Prakah-Asante K.O. (Craig K.C.)**,** 1992: "An Investigation of the Effects of Backlash, Coulomb Friction and Joint Compliance on the Dynamics and Control of a Mechanical Positioning System." *R.P.I. Department of Mechanical Engineering, Aeronautical Engineering and Mechanics*, Master of Science Thesis.

Prakah-Asante K.O., Islam A.S., Walczyk D.F., and Craig K.C., 1993: "Design, Construction and Testing of a Single-Axis Servomechanism for Control Experiments involving Coulomb Friction, Backlash and Joint Compliance." *Journal of Engineering Design*, vol.4 no.4 pp.305-329.

Tao G. and Kokotovic V., 1993: "Adaptive Control of Systems with Backlash." *Automatica.*

Thomson W.T., 1993: Theory of Vibrations, ed.4 (Prentice-Hall).

Tung E.D., Anwar G., and Tomizuka M., 1993: "Low-Velocity Friction Compensation and Feedforward Solution based on Repetitive Control." *Journal of Dynamic Systems, Measurement, and Control*, vol.115 (June) pp.279-284.

Walczyk D.F. (Craig K.C.), 1991: "Design and Implementation of an Experimental Computer-Controlled Single-Axis Manipulator." *R.P.I. Department of Mechanical Engineering, Aeronautical Engineering and Mechanics*, Master of Science Thesis (Aug.).

de Wit C.C., Noel P., and Aubin A., 1991: "Adaptive Friction Compensation in Robotic Manipulators: Low Velocities." *The International Journal of Robotics Research*, vol.10 no.3 (Jun.) pp.189-199.

Yang Y.P. and Chu J.S., 1993: "Adaptive Velocity Control of DC Motors with Coulomb Friction Identification." *Journal of Dynamic Systems, Measurement, and Control*, vol.115 no.3 (Mar.) pp.95-102.

Yuh J. and Tissue D.K., 1991: "Discrete-Time Adaptive Control for Mechanical Manipulators having a Joint Compliance." *Journal of Robotic Systems*, vol.8 no.6 (Dec.) pp.745-765.